Short-range order, atomic displacements and effective interatomic ordering energies in TiN0.82

T. Priem, B. Beuneu, C.H. de Novion, A. Finel, F. Livet

▶ **To cite this version:**

T. Priem, B. Beuneu, C.H. de Novion, A. Finel, F. Livet. Short-range order, atomic displacements and effective interatomic ordering energies in TiN0.82. Journal de Physique, 1989, 50 (16), pp.2217-2242. 10.1051/jphys:0198900500160221700 . jpa-00211056

HAL Id: jpa-00211056
https://hal.science/jpa-00211056v1

Submitted on 4 Feb 2008

HAL is a multi-disciplinary open access archive for the deposit and dissemination of scientific research documents, whether they are published or not. The documents may come from teaching and research institutions in France or abroad, or from public or private research centers.

L'archive ouverte pluridisciplinaire **HAL**, est destinée au dépôt et à la diffusion de documents scientifiques de niveau recherche, publiés ou non, émanant des établissements d'enseignement et de recherche français ou étrangers, des laboratoires publics ou privés.

J. Phys. France **50** (1989) 2217-2242 15 AOÛT **1989,** PAGE 2217

Classification
Physics Abstracts
61.60 — 61.70B — 64.60

Short-range order, atomic displacements and effective interatomic ordering energies in $TiN_{0.82}$ (*)

T. Priem (1), B. Beuneu (1), C. H. de Novion (1), A. Finel (2) and F. Livet (3)

(1) C.E.A./IRDI/DMECN/DTech., Laboratoire des Solides Irradiés, Ecole Polytechnique, 91128 Palaiseau Cedex, France
(2) O.M./ONERA, BP 72, 92322 Chatillon Cedex, France
(3) Laboratoire de Thermodynamique et Physico-Chimie Métallurgiques, I.N.P.G., BP 75, 38402 Saint Martin d'Hères, France

(*Reçu le 5 octobre 1988, révisé le 26 avril 1989, accepté le 27 avril 1989*)

Résumé. — La section efficace de diffusion diffuse élastique de neutrons par un monocristal $TiN_{0,82}$ a été mesurée à l'équilibre thermodynamique à 700, 800 et 900 °C. L'intensité diffuse est maximale aux points de type (1/2 1/2 1/2) du réseau réciproque. Les lacunes d'azote se mettent préférentiellement en positions de 3es voisins sur le sous-réseau métalloïde c.f.c. Des énergies effectives de mise en ordre de paires d'atomes ont été calculées, par l'approximation de champ moyen, par simulations de Monte-Carlo et par la Méthode de Variation d'Amas ; les deux dernières techniques ont donné des énergies très proches, indépendantes de la température : $V_1 \simeq 82$ et $V_2 \simeq 62$ meV pour les premiers et seconds voisins azote respectivement ; V_3 et les énergies d'interaction plus lointaines sont très faibles. Les atomes de titane s'éloignent, et les atomes d'azote se rapprochent de leurs lacunes premières voisines, de 0,042 et 0,024 Å respectivement.

Abstract. — The elastic diffuse neutron scattering of a $TiN_{0.82}$ single crystal has been measured in thermodynamic equilibrium at 700, 800 and 900 °C. The diffuse intensity is maximum at the (1/2 1/2 1/2) type reciprocal lattice positions. Nitrogen vacancies are found to situate preferentially as third neighbours on the metalloid f.c.c. sublattice. Pair interaction ordering energies were calculated by mean-field approximation, Monte-Carlo simulations, and Cluster Variation Method ; the last two methods give very similar temperature independent pair energies : $V_1 \simeq 82$ and $V_2 \simeq 62$ meV for first and second nitrogen neighbours respectively ; V_3 and further interaction energies are very small. Titanium atoms are found to relax away, and nitrogen atoms to relax toward their first neighbour vacancies, by respectively 0.042 and 0.024 Å.

(*) Experiment performed at Laboratoire Léon Brillouin (laboratoire commun CEA-CNRS), Saclay, France.

Article published online by EDP Sciences and available at http://dx.doi.org/10.1051/jphys:01989005001602217 00

1. Introduction.

Titanium mononitride TiN_x is a metallic compound with the f.c.c. NaCl type crystal structure. It shows extreme hardness, a high melting point (up to 2 950 °C for $x = 1$) and superconductivity ($T_c = 5.49$ K for stoichiometric TiN) [1]. TiN has important applications as thin films and coatings for mechanical wear resistance of cutting tools.

TiN_x displays large departures from the stoichiometric composition, and can be found with a nitrogen concentration x between 0.5 and 1.15. Non-stoichiometry is accommodated by nitrogen vacancies for $0.5 < x < 1$ and by titanium vacancies for $x > 1$ [1]. It has been shown that these vacancies affect thermodynamic, mechanical, electrical, magnetic and superconducting properties. For example, (i) the superconducting critical temperature decreases with vacancy concentration, (ii) the lattice parameter a_{fcc} increases with nitrogen concentration for $x < 1$, attains a maximum value 4.24 Å for stoichiometric TiN, and then decreases for $x > 1$ [1].

In transition metal carbides and nitrides, vacancies are not randomly distributed, but are organized in a long or short-range order. Furthermore, vacancies induce also small local distortions of the lattice. Experimentally, the short-range order (SRO) and the local distortions give rise to a diffuse intensity in the electron, X-ray or neutron scattering spectra, which has been observed [2]. In particular, Billingham *et al.* [3] have seen electron diffuse scattering surfaces in TiN_x for x between 0.5 and 0.75 ; this observation, later extended to $0.65 \leqslant x < 0.88$ by Nagakura and Kusunoki [4], has been tentatively explained by a short-range order model [5]. However, (i) electron scattering does not allow quantitative measurements of the diffuse intensity, (ii) X-ray measurements in $NbC_{0.72}$ [6] and elementary considerations on scattering amplitudes ($|f_{Metal}| \gg |f_N|, |f_C|$) show that X-ray and electron diffuse intensities are dominated by metallic atom displacements. Neutrons are therefore necessary to study the short-range order of metalloid atoms in transition metal carbides and nitrides.

At low nitrogen content ($0.5 \leqslant x \leqslant 0.61$), TiN_x annealed below 800 °C shows a δ'-Ti_2N superstructure of space group $I4_1/amd$, where nitrogen vacancies are long-range ordered (LRO). This superstructure is characterized by (1 1/2 0) diffraction spots in the reciprocal lattice [2, 4, 7, 8]. δ'-Ti_2N is metastable, as at 750 °C, the following phase transformation sequence was directly observed by neutron diffraction [9] :

$$\text{Quenched} \quad \delta\text{-}TiN_x \rightarrow \delta + \delta' \rightarrow \delta'\text{-}Ti_2N \rightarrow \delta' + \delta + \varepsilon \rightarrow \delta\text{-}TiN_{0.65} + \varepsilon Ti_2N ,$$

where δ = disordered rocksalt structure TiN_x, and ε-Ti_2N is a stable phase with the tetragonal antirutile structure [10] (1).

A theoretical work has recently been undertaken to understand this vacancy ordering in transition metal nitrides and carbides from their band structure. Calculations based on the generalized perturbation method and in the coherent potential approximation were developed by Landesman *et al.* [13, 14]. These authors used an Ising model where only pair interactions are taken into account, and assumed temperature equal to 0 K, the lattice rigid and the transfer integrals independent of concentration x. The calculations gave the effective ordering pair energies V_n (defined precisely in Sect. 5) between n-th neighbour metalloid sites *versus* the relative filling N_e of metal 3d-metalloid 2p bands (see Fig. 1). These energies decrease

(1) Two other TiN_x phases in the composition range $0.3 \leqslant x \leqslant 0.5$ have been recently discovered [11, 12].

rapidly with distance, so that for $n \geqslant 5$ they are negligible. For $TiN_{0.82}$, $N_e = \frac{4+3x}{10+6x} = 0.43$, and one obtains from figure 1 :

$$V_1 = 38 \text{ meV} , \quad V_2 = 227 \text{ meV} , \quad V_3 = -4 \text{ meV} , \quad V_4 = -19 \text{ meV} .$$

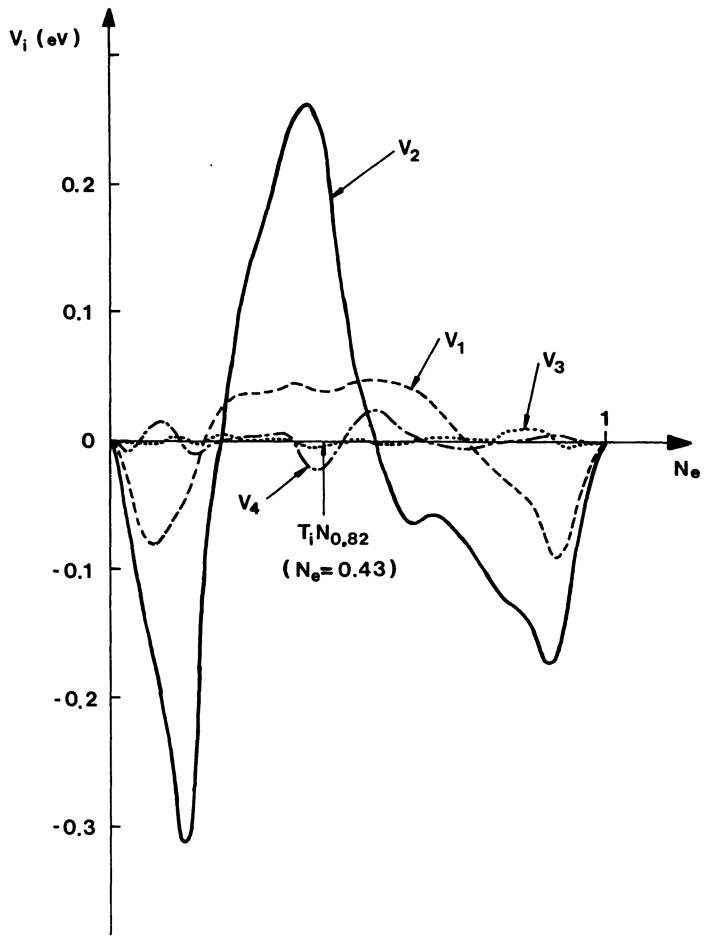

Fig. 1. — Pair interaction energies V_i *versus* band filling N_e for transition metal nitrides M_6N_5, calculated by the generalized perturbation method (G. Treglia, private communication).

The short-range order structure of $TiN_{0.82}$ can be predicted from the stability diagrams of Clapp and Moss [15, 16] mean field approximation depicted in figure 2 : from the above V_1, V_2 and V_3 energies, it is found in the (1/2 1/2 1/2) field, i.e. the diffuse intensity is predicted to be maximum at the (1/2 1/2 1/2) type positions in the reciprocal lattice.

On the other hand, the theoretical calculations mentioned above did not succeed to explain the occurrence of the LRO (1 1/2 0) δ'-Ti_2N phase, which requires $V_1 \gtrsim 2\,V_2 \gtrsim 0$ (if V_3 is small). The same difficulty was encountered in a theoretical calculation based on the recursive method [13] : even by varying the input tight-binding parameters (within physically

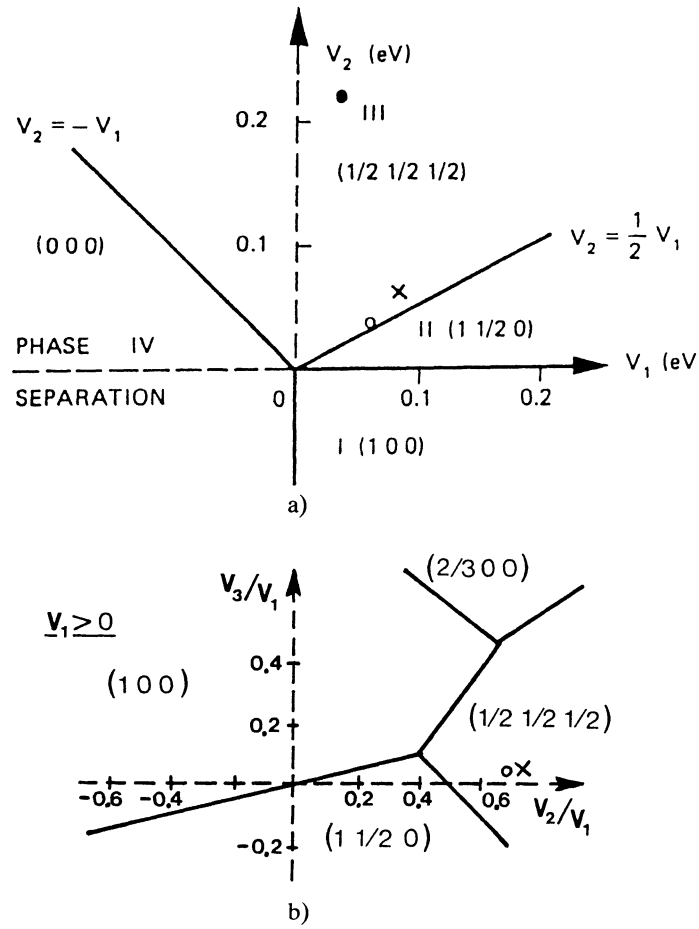

Fig. 2. — Clapp and Moss stability diagrams of short-range order in f.c.c. solid solutions [16] a) *versus* V_1 and V_2 ($V_3 = 0$) ; b) *versus* V_2/V_1 and V_3/V_1. In each region is indicated the point of the reciprocal lattice where the diffuse intensity is maximum. Representative points for $TiN_{0.82}$: (•) theoretical calculation by the generalized perturbation method (from Fig. 1), (○) from analysis of present neutron diffuse scattering data by the Clapp and Moss formula, (×) idem, by Monte-Carlo and inverse CVM methods.

reasonable limits), the δ'-Ti_2N phase could only be found stable in a narrow electron concentration range ($N_e \simeq 0.5$), with a very small stability energy.

The problem is now to determine experimentally the short-range order of $TiN_{0.82}$ and the values of the pair interaction potentials. Preliminary diffuse neutron scattering data on powder samples TiN_x [17] gave rather unphysical results (negative first four SRO coefficients, see Sect. 6). In [18], we have found, by neutron scattering at room temperature on a $TiN_{0.82}$ single crystal (in a quenched state) maxima of diffuse intensity in (1/2 1/2 1/2). In neutron scattering experiments, the strong high temperature phonon scattering can be eliminated by energy analysis ; for this reason, the diffuse scattering experiments can be carried in the region of the phase diagram where the system is disordered and where high temperature fluctuations are in thermodynamic equilibrium (thus avoiding the quenching

problem of samples). In the present work, the short-range order parameters $\alpha_{\ell mn}$ and the mean static atomic displacements have been determined for the same $TiN_{0.82}$ single crystal, *in situ,* at 700, 800 and 900 °C. Then the pair interaction energies were calculated by three different methods (Clapp and Moss mean-field approximation, Monte-Carlo simulation and Inverse Cluster Variation Method).

2. Experimental.

The $TiN_{0.82}$ single crystal was prepared by a zone-annealing technique [19]. Details on sample characterization are given in reference [18].

The diffuse neutron scattering experiment was performed at three temperatures (T = 700 °C, 800 °C, 900 °C) on the two axis spectrometer G4-4 [20] at Laboratoire Léon Brillouin ([2]), C.E.N.-Saclay, France. The $\{001\}$ and $\{1\bar{1}0\}$ planes of the reciprocal lattice were explored with an incident wavelength λ = 2.56 Å (resolution $\Delta\lambda/\lambda \leqslant 4 \times 10^{-2}$). The sample was in a vacuum chamber ($\sim 10^{-6}$ torr). 48 He^3 detectors of diameter 50 mm with time-of-flight analysis and rotation ω of the sample, allowed to obtain the elastic diffuse cross-section for :

$0.5 \leqslant Q = 4\,\pi \sin\theta\ /\lambda \leqslant 4.5$ Å^{-1} with steps 2.5° in 2θ and 3° in ω. The furnace was a niobium foil heater.

The data were calibrated to absolute units by comparison with a vanadium standard after background correction, and were corrected for effective absorption, total incoherent scattering and Debye-Waller factor, as described below.

The intensity in the two reciprocal planes is calculated in Laüe units (1 Laüe = $x(1-x)\,b_N^2$ = 0.130 barns, see Sect. 3) by the formula :

$$\frac{d\sigma}{d\Omega} = C\,\frac{I_{TiN} - I_{Vac} + (1-\alpha_{TiN})(I_{Vac} - I_{BN})}{I_V - I_{Vac} + (1-\alpha_V)(I_{Vac} - I_{BN})} - \frac{d\sigma_{inc}}{d\Omega} \qquad (1)$$

where :

- I_{TiN}, I_V, I_{BN}, I_{Vac} are respectively the numbers of detected neutrons when sample, vanadium standard, boron nitride (neutron absorbant) and vacuum are in the beam.
- α_{TiN} and α_V are the effective transmission coefficients for $TiN_{0.82}$ and vanadium (due to nuclear absorption + incoherent + Laüe scattering) : $\alpha_{TiN} = 0.46$ and $\alpha_V = 0.57$ for λ = 2.56 Å (calculated from the data of Ref. [21]).
- C is a normalization coefficient which has the following expression :

$$C = \frac{\alpha_V\, N_V(\sigma_V^{inc} + \sigma_V^{MS})\, e^{-2B_V \sin^2\theta/\lambda^2}}{\alpha_{TiN}\, N_{Ti}\, x(1-x)\, \sigma_N^{coh}\, e^{-2B_{TiN}\sin^2\theta/\lambda^2}}$$

- $\frac{d\sigma_{inc}}{d\Omega}$ is the incoherent differential cross-section in Laüe units :

$$\frac{d\sigma_{inc}}{d\Omega} = \frac{\sigma_{Ti}^{inc} + x\sigma_N^{inc} + \sigma_{TiN}^{MS}}{x(1-x)\,\sigma_N^{coh}} = 2.22 \text{ Laüe } (0.29 \text{ barn}) \text{ per Ti atom [21]}.$$

([2]) Laboratoire commun CEA-CNRS.

σ_x^{coh}, σ_x^{inc} and σ_x^{MS} are the coherent, incoherent and total multiple scattering cross-sections (the multiple scattering cross-section was calculated by the method of Blech and Averbach [22]).

N_{Ti} and N_V are the numbers of titanium and vanadium atoms in the beam.

B_{TiN} and B_V are the Debye-Waller factors for titanium nitride and vanadium ($B_{TiN} \simeq B_{Ti} \simeq B_N = 0.82$ Å^2 for $T = 700$ °C, 0.89 Å^2 for $T = 800$ °C, 0.97 Å^2 for $T = 900$ °C [23], $B_V = 0.57$ Å^2 at 300 K [24]).

The inelastically scattered neutrons are due to the interaction with the phonons. The energy resolution in our experimental conditions was $\Delta E \simeq 25$ meV for phonon annihilation and 7 meV for phonon creation : for most of the time-of-flight spectra, it is relatively easy to separate the elastic and the non-elastic neutrons (Fig. 3) ; in particular, the optical phonons (60-80 meV) and the acoustical phonons near the Brillouin zone border (30-40 meV) are eliminated. Nevertheless, close to the Bragg reflexions, as the phonon energies are low, the separation between the phonon scattering and the elastic scattering cannot be done. By comparison with the phonon spectrum of TiN [25], one can deduce that the low energy acoustic phonons are not separated within a zone of dimensions $\simeq 0.2$-0.3 (in h_1, h_2, h_3 units) around the Bragg peaks. This is the zone where abnormally high intensities are observed (Fig. 4) ; the corresponding data had to be eliminated in the least squares fit ([3]).

The normalization factors C (for Eq. (1)) of both experiments in the $\{001\}$ and $\{1\bar{1}0\}$ planes, are adjusted in order to obtain the same diffuse intensity along the common line of the two planes (the correction, due to uncertainties on the values of N_V, N_{Ti}, α_V, α_{TiN}, is about 10 %).

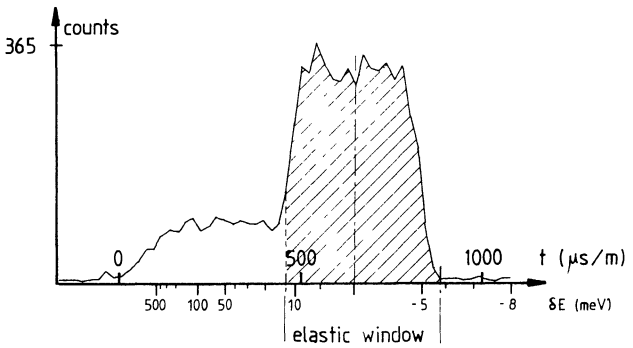

Fig. 3. — Number of counted neutrons *versus* time-of-flight per meter and energy transfer to the neutron recorded in a He^3 detector on spectrometer G4-4, Orphée reactor, Saclay, for $TiN_{0.82}$ at 900 °C.

3. Results.

Preliminary thermal cycles without time-of-flight were carried out between 700 and 900 °C. They have shown that the diffuse intensity is reversible with temperature and that the nitrogen sublattice is in thermodynamic equilibrium within a few minutes in this temperature range.

([3]) A high resolution energy experiment at room temperature, performed on spectrometer D7, I.L.L., Grenoble, confirmed that the large diffuse intensity observed in $TiN_{0.82}$ close to the Bragg peaks is an inelastic scattering.

The elastic diffuse differential cross-section $d\sigma/d\Omega$ of $TiN_{0.82}$ for two temperatures $T = 700$ °C and 900 °C, measured with time-of-flight analysis, is shown in figure 4. (For $T = 800$ °C, the spectrum has an intermediary shape between the 700 and 900 °C ones.)

- In the {001} plane, the diffuse intensity is concentrated along circles centered on the reciprocal node (110). No maxima are observed at the Ti_2N superlattice reflexion positions (1 1/2 0).
- In the $\{1\bar{1}0\}$ plane, the diffuse intensity streaks are roughly parallel to the ⟨001⟩ direction. The intensity is maximum at the (1/2 1/2 1/2) type positions.
- The high temperature spectra have the same shape as for the quenched sample studied in [18]. Diffuse scattering is concentrated on the surface observed by electron diffraction, but the intensity is far to be constant along this surface and far to be periodic in the reciprocal lattice.
- The maxima of the diffuse intensity decrease with increasing temperature.

The elastic diffuse scattering intensity contains two terms. The first one is the short-range order contribution, periodic in the reciprocal lattice. The second one is the non periodic contribution of the static atomic displacements. In $TiN_{0.82}$, the two terms have a comparable importance.

Expanded up to the second order with respect to the static displacements, which are much smaller than a_{fcc}, the elastic diffuse cross-section for TiN_x has the following expression [26] :

$$\frac{d\sigma}{d\Omega}(h_1, h_2, h_3) = \mathcal{N} x(1-x)\, b_N^2 \Bigg[\sum_{\substack{\ell, m, n \in \mathbf{Z} \\ \ell+m+n \text{ even}}} \alpha_{\ell mn} \cos(\pi h_1 \ell) \cos(\pi h_2 m) \cos(\pi h_3 n)$$

$$+ \sum_{\ell, m, n \in \mathbf{Z}} \gamma_{\ell mn} [h_1 \sin(\pi h_1 \ell) \cos(\pi h_2 m) \cos(\pi h_3 n)$$

$$+ h_2 \sin(\pi h_2 \ell) \cos(\pi h_3 m) \cos(\pi h_1 n) + h_3 \sin(\pi h_3 \ell) \cos(\pi h_1 m) \cos(\pi h_2 n)]$$

$$+ \sum_{\ell, m, n \in \mathbf{Z}} \delta_{\ell mn} [h_1^2 \cos(\pi h_1 \ell) \cos(\pi h_2 m) \cos(\pi h_3 n)$$

$$+ h_2^2 \cos(\pi h_2 \ell) \cos(\pi h_3 m) \cos(\pi h_1 n) + h_3^2 \cos(\pi h_3 \ell) \cos(\pi h_1 m) \cos(\pi h_2 n)]$$

$$+ \sum_{\ell, m, n \in \mathbf{Z}} \varepsilon_{\ell mn} [h_1 h_2 \sin(\pi h_1 \ell) \sin(\pi h_2 m) \cos(\pi h_3 n)$$

$$+ h_1 h_3 \sin(\pi h_1 \ell) \sin(\pi h_3 m) \cos(\pi h_2 n) + h_2 h_3 \sin(\pi h_2 \ell) \sin(\pi h_3 m) \cos(\pi h_1 n)] \Bigg]$$

where :

- ℓ, m, n are the coordinates of the ideal atomic positions in the crystal :

$$\mathbf{R}_{\ell mn} = \ell \frac{\mathbf{a}}{2} + m \frac{\mathbf{b}}{2} + n \frac{\mathbf{c}}{2}$$

(**a**, **b**, **c** unit vectors of the f.c.c. cell).

- h_1, h_2, h_3 are the coordinates of the scattering vector **Q** in the reciprocal lattice (of unit vectors **a***, **b***, **c***) :

$$\mathbf{Q} = 2\pi (h_1 \mathbf{a}^* + h_2 \mathbf{b}^* + h_3 \mathbf{c}^*) .$$

- $\alpha_{\ell mn}$ is the Cowley-Warren SRO coefficient : $\alpha_{\ell mn} = 1 - \dfrac{P_{\ell mn}}{1-x}$, where $P_{\ell mn}$ is the

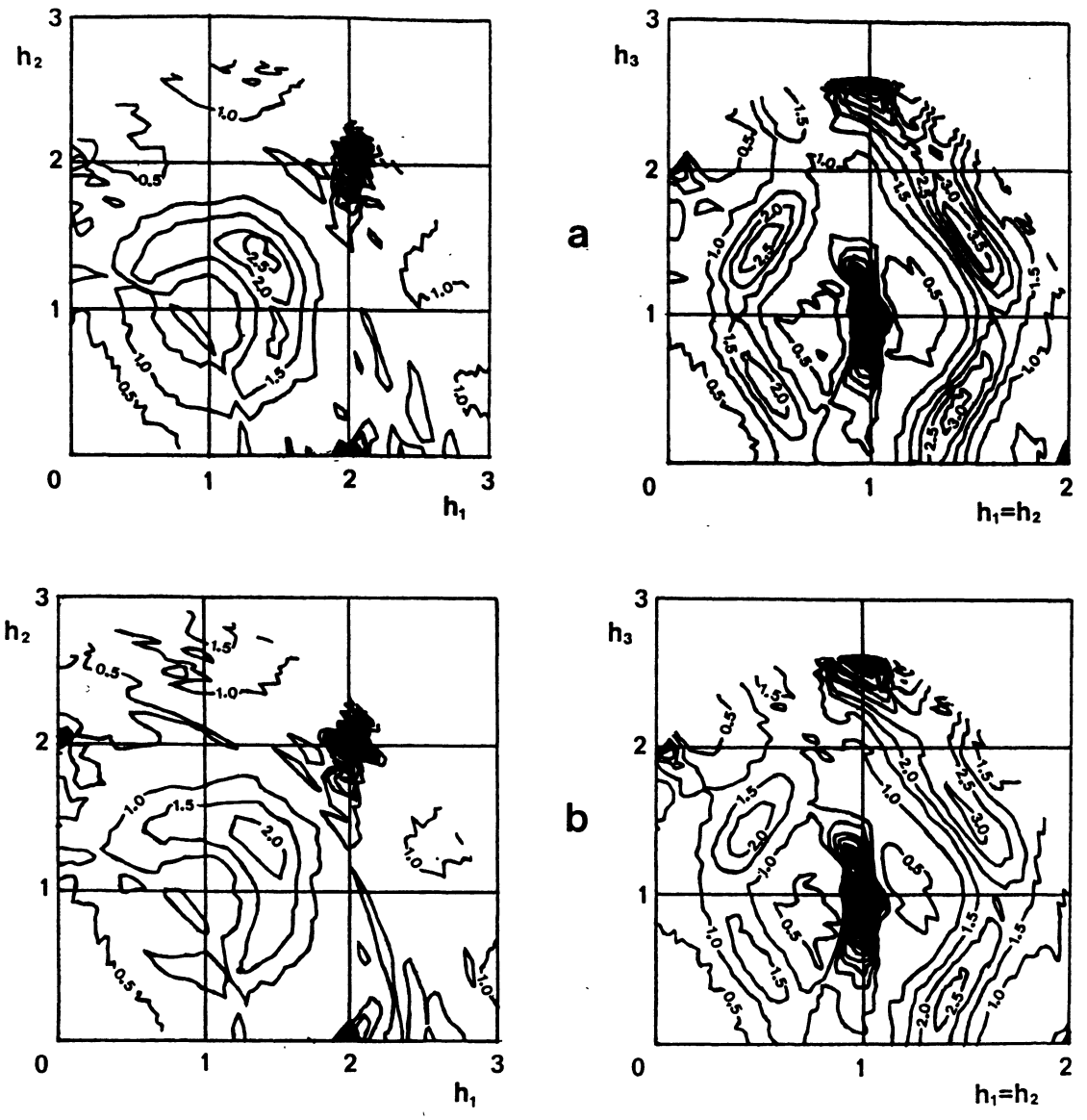

Fig. 4. — Elastic diffuse intensity (in Laüe units) for the reciprocal planes {001} (left) and $\{1\bar{1}0\}$ (right) of $TiN_{0.82}$, measured at high temperature by neutron scattering. a) $T = 700$ °C, b) $T = 900$ °C, c) reconstructed cross-section from the fit parameters for $T = 700$ °C. Bragg peaks are found at $h_1 = h_2 = h_3 = 1$; $h_1 = 2$, $h_2 = h_3 = 0$; $h_1 = h_2 = 2$, $h_3 = 0$; etc...

conditional probability to find a vacancy at the (ℓ, m, n) lattice position, if a nitrogen is at the origin.

$$\bullet \gamma_{\ell mn} = -\pi \left(\frac{x}{1-x} + \alpha_{\ell mn} \right) \langle L^{\text{N-N}}_{\ell mn} \rangle \quad \text{if} \quad \ell + m + n \quad \text{even}$$

$$= -\frac{2\pi b_{\text{Ti}}}{(1-x)\, b_{\text{N}}} \langle L^{\text{Ti-N}}_{\ell mn} \rangle \quad \text{if} \quad \ell + m + n \quad \text{odd}$$

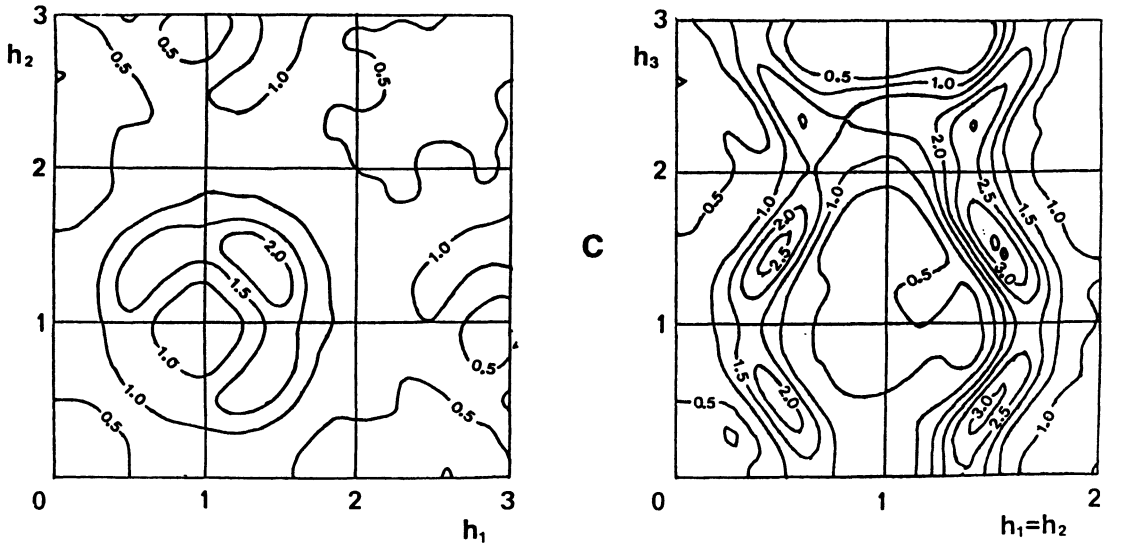

Figure 4 (*continued*).

$$\bullet\,\delta_{\ell mn} = -\frac{\pi^2}{2}\left(\frac{x}{1-x} + \alpha_{\ell mn}\right)\left\langle (L_{\ell mn}^{\text{N-N}})^2\right\rangle - \frac{\pi^2 b_{\text{Ti}}^2}{2x(1-x)\,b_{\text{N}}^2}\left\langle (L_{\ell mn}^{\text{Ti-Ti}})^2\right\rangle \quad \text{if} \quad \ell+m+n \quad \text{even}$$

$$= -\frac{\pi^2 b_{\text{Ti}}}{(1-x)\,b_{\text{N}}}\left\langle (L_{\ell mn}^{\text{Ti-N}})^2\right\rangle \quad \text{if} \quad \ell+m+n \quad \text{odd}$$

$$\bullet\,\varepsilon_{\ell mn} = +\pi^2\left(\frac{x}{1-x} + \alpha_{\ell mn}\right)\left\langle L_{\ell mn}^{\text{N-N}} M_{\ell mn}^{\text{N-N}}\right\rangle +$$

$$+\frac{\pi^2 b_{\text{Ti}}^2}{x(1-x)\,b_{\text{N}}^2}\left\langle L_{\ell mn}^{\text{Ti-Ti}} M_{\ell mn}^{\text{Ti-Ti}}\right\rangle \quad \text{if} \quad \ell+m+n \quad \text{even}$$

$$= +\frac{2\pi^2 b_{\text{Ti}}}{(1-x)\,b_{\text{N}}}\left\langle L_{\ell mn}^{\text{Ti-N}} M_{\ell mn}^{\text{Ti-N}}\right\rangle \quad \text{if} \quad \ell+m+n \quad \text{odd}\,.$$

$L_{\ell mn}^{\text{A-B}}$ and $M_{\ell mn}^{\text{A-B}}$ represent the components along **a** and **b** of the relative displacement $\mathbf{u}_{\ell mn}$ of A and B atoms separated by $\mathbf{R}_{\ell mn}$

$$\mathbf{u}_{\ell mn} = L_{\ell mn}\frac{\mathbf{a}}{2} + M_{\ell mn}\frac{\mathbf{b}}{2} + N_{\ell mn}\frac{\mathbf{c}}{2}$$

$\langle \cdots \rangle$ represents the space average of the quantity into brackets.

• $\mathcal{N}$ = number of Ti atoms, b_{N} and b_{Ti} = scattering amplitudes of N and Ti (respectively $+0.94 \times 10^{-12}$ cm and -0.34×10^{-12} cm [21]).

The $\alpha_{\ell mn}$, $\gamma_{\ell mn}$ and $\delta_{\ell mn}$ parameters have been determined from the experimental cross-section $\mathrm{d}\sigma/\mathrm{d}\Omega$ by the least-squares method.

Due to low energy phonon scattering (see Sect. 2), measurements in small spheres of the reciprocal lattice close to the Bragg peaks (radius 0.3 in h_i units) had to be eliminated from the fit.

In the fit, the condition $\sum_{\ell mn} \alpha_{\ell mn} = 0$ (including α_{000}) has been assumed ; if not, too many values of $\alpha_{\ell mn}$ were negative without any physical meaning (negative diffuse intensity at the

Bragg peaks !). In fact, from statistical models, the sum of the short-range order parameters can vary between 0 and 1 (0 in the canonical system, 1 in the grand-canonical system). In any case, in the least-squares fit, the calculated parameters do not differ significantly if we modify the value of K ($0 \leqslant K \leqslant 1$) in the condition $\sum_{\ell mn} \alpha_{\ell mn} = K$.

The fit was made with several sets of $\alpha_{\ell mn}$, $\gamma_{\ell mn}$ and $\delta_{\ell mn}$ parameters. As shown in table I, the first $\alpha_{\ell mn}$ and $\gamma_{\ell mn}$ values were found practically insensitive to the number of parameters chosen for the fit. The second order contribution is very small, and as can be seen in table I, the introduction of $\delta_{\ell mn}$ parameters does not influence much the $\alpha_{\ell mn}$ and $\gamma_{\ell mn}$ values ; only two $\delta_{\ell mn}$ have been considered. Contrary to $\gamma_{\ell mn}$, the $\delta_{\ell mn}$ increase with temperature, which means that they incorporate some phonon scattering. The $\varepsilon_{\ell mn}$ parameters do not appear because the first ones (ε_{001} and ε_{100}) are equal to zero by symmetry.

Table I. — *Effect of the number of parameters of the fit on the first* $\alpha_{\ell mn}$ *and* $\gamma_{\ell mn}$ (700 °C).

	4 α + 1 γ	12 α + 8 γ	17 α + 14 γ	25 α + 19 γ	25 α + 19 γ + 2 δ
α_{000}	1.132	1.128	1.129	1.121	1.127
α_{011}	− 0.089	− 0.104	− 0.102	− 0.103	− 0.105
α_{002}	− 0.110	− 0.122	− 0.123	− 0.121	− 0.118
α_{112}	0.029	0.045	0.046	0.047	0.047
	−	0.021	0.021	0.020	0.019
α_{013}	−	0.022	0.021	0.021	0.020
α_{222}	−	− 0.021	− 0.027	− 0.028	− 0.029
α_{123}	−	− 0.014	− 0.019	− 0.019	− 0.019
γ_{100}	− 0.072	− 0.057	− 0.059	− 0.060	− 0.059
γ_{110}	−	− 0.027	− 0.027	− 0.026	− 0.026
γ_{111}	−	0.023	0.023	0.025	0.024
γ_{200}	−	0.029	0.025	0.023	0.023

Data in the two reciprocal planes $\{001\}$ and $\{1\bar{1}0\}$ have been used. These data lead to a least-squares fit matrix of rank equal to the number of unknown parameters. The $\alpha_{\ell mn}$, $\gamma_{\ell mn}$ and $\delta_{\ell mn}$ with $\langle L_{\ell mn} \rangle$ and $\langle L^2_{\ell mn} \rangle$ values (from the fit with 24 α, 19 γ and 2 δ) are given in tables II and III.

In fact, the fit was made using the data of every two detectors and every two rotations ω of the sample. The four sets of parameters obtained gave an estimate of the statistical errors from experimental data : these statistical errors for $\alpha_{\ell mn}$ are given in table II.

The reconstructed cross-sections from the fitted parameters are shown in figure 4.

The fit gave $\alpha_{000} \simeq 1.06$ to 1.15, instead of 1, the theoretical value. This discrepancy is mainly due to the difficulties to determine exactly the real number of atoms of the sample in the neutron beam and the transmission coefficient. If the error on the value of the incoherent cross-section $\mathrm{d}\sigma_{\mathrm{inc}}/\mathrm{d}\Omega$ is assumed negligible, this discrepancy may be interpreted as a scale factor for the cross-section unit. For this reason, the $\alpha_{\ell mn}$, $\gamma_{\ell mn}$ and $\delta_{\ell mn}$ parameters have been corrected by means of the following equation :

$$\alpha_{\ell mn}^{\text{corrected}} = \alpha_{\ell mn}^{\text{non corrected}} \left(\frac{1 + \mathrm{d}\sigma_{\mathrm{inc}}/\mathrm{d}\Omega}{\alpha_{000}^{\text{non corrected}} + \mathrm{d}\sigma_{\mathrm{inc}}/\mathrm{d}\Omega} \right) . \qquad (2)$$

Table II. — *Non corrected* $\alpha_{\ell mn}$ *parameters and estimate of the statistical error (into brackets) for* $T = 700$, 800 *and* 900 °C. *For* $T = 700$ °C *are also given the measured* $\alpha_{\ell mn}$ *parameters corrected by formula* (2), *and the* $\alpha_{\ell mn}$ *calculated by Monte-Carlo from the four* M.C. V_i *of table* V.

$\alpha_{\ell mn}$	$T = 900$ °C non corrected	$T = 800$ °C non corrected	$T = 700$ °C non corrected	$T = 700$ °C corrected	$T = 700$ °C from Monte Carlo V_i
α_{000}	1.069 (15)	1.103 (18)	1.127 (10)	1	1
α_{011}	− 0.092 (2)	− 0.098 (2)	− 0.105 (2)	− 0.101 (2)	− 0.101
α_{002}	− 0.098 (5)	− 0.102 (5)	− 0.118 (5)	− 0.114 (5)	− 0.114
α_{112}	0.035 (2)	0.040 (2)	0.047 (2)	0.045 (2)	0.045
α_{022}	0.013 (3)	0.013 (3)	0.019 (3)	0.018 (3)	0.017
α_{013}	0.015 (1)	0.017 (1)	0.020 (1)	0.019 (1)	0.018
α_{222}	− 0.018 (1)	− 0.024 (1)	− 0.029 (1)	− 0.028 (1)	− 0.019
α_{123}	− 0.014 (1)	− 0.015 (1)	− 0.019 (1)	− 0.018 (1)	− 0.015
α_{004}	− 0.005 (3)	− 0.000 (3)	0.003 (3)	0.003 (3)	0.009
α_{033}	0.003 (1)	0.000 (1)	− 0.002 (1)	− 0.002 (1)	0.001
α_{114}	− 0.005 (1)	− 0.008 (1)	− 0.010 (1)	− 0.010 (1)	− 0.010
α_{024}	0.004 (1)	0.004 (1)	0.003 (1)	0.003 (1)	− 0.001
α_{233}	0.008 (1)	0.010 (1)	0.013 (1)	0.013 (1)	0.008
α_{224}	0.005 (1)	0.008 (1)	0.010 (1)	0.010 (1)	0.007
α_{015}	− 0.002 (1)	− 0.001 (1)	− 0.001 (1)	− 0.001 (1)	− 0.001
α_{134}	0.002 (1)	0.003 (1)	0.004 (1)	0.004 (1)	0.003
α_{125}	− 0.001 (1)	− 0.001 (1)	0.000 (1)	0.000 (1)	0.003
α_{044}	0.003 (2)	0.002 (2)	0.002 (2)	0.002 (2)	− 0.001
α_{035}	0.000 (1)	0.000 (1)	0.000 (1)	0.000 (1)	− 0.001
α_{334}	− 0.001 (1)	− 0.003 (1)	− 0.004 (1)	− 0.004 (1)	− 0.004
α_{006}	− 0.003 (2)	− 0.001 (2)	0.000 (2)	0.000 (2)	0.000
α_{244}	− 0.003 (1)	− 0.004 (1)	− 0.005 (1)	− 0.005 (1)	− 0.003
α_{116}	0.004 (1)	0.003 (1)	0.003 (1)	0.003 (1)	0.000
α_{235}	− 0.002 (1)	− 0.002 (1)	− 0.002 (1)	− 0.002 (1)	− 0.003
α_{026}	− 0.001 (1)	− 0.002 (1)	− 0.003 (1)	− 0.003 (1)	− 0.001

The correction is about 3×10^{-3} on the first neighbour α_{011} parameter, and less for the following $\alpha_{\ell mn}$; the corrected $\alpha_{\ell mn}$ parameters are given in table II for $T = 700$ °C.

4. Atomic displacements.

As can be seen in figure 4, for $TiN_{0.82}$ the contribution of the atomic displacements to the diffuse intensity is not negligible (the intensity maps are not periodic in the reciprocal lattice) ; this contribution is shown in figure 5 for $T = 700$ °C. From table III, the static atomic displacements $\langle L \rangle$ are seen to be independent of temperature.

The average atomic displacements around a vacancy $\langle L_{\ell mn}^{\square\text{-A}} \rangle$ (A = Ti or N) are determined from the $\langle L_{\ell mn}^{\text{N-A}} \rangle$ by the relations :

$$0.82 \langle L_{\ell mn}^{\text{N-Ti}} \rangle + 0.18 \langle L_{\ell mn}^{\square\text{-Ti}} \rangle = 0 \quad \text{if} \quad \ell + m + n \text{ odd} ,$$

$$(0.82 + 0.18\, \alpha_{\ell mn}) \langle L_{\ell mn}^{\text{N-N}} \rangle + 0.36 (1 - \alpha_{\ell mn}) \langle L_{\ell mn}^{\square\text{-N}} \rangle = 0 \quad \text{if} \quad \ell + m + n \quad \text{even} .$$

Table III. — *Values of* $\gamma_{\ell mn}$, $\delta_{\ell mn}$, $\langle L_{\ell mn} \rangle$ *and* $\langle L^2_{\ell mn} \rangle$ *for* $T = 700$, 800 *and* 900 °C.

ℓmn	$T = 700$ °C		$T = 800$ °C		$T = 900$ °C	
	$\gamma_{\ell mn}$	$\langle L_{\ell mn} \rangle$ 10^{-3} $(a/2)$	$\gamma_{\ell mn}$	$\langle L_{\ell mn} \rangle$ 10^{-3} $(a/2)$	$\gamma_{\ell mn}$	$\langle L_{\ell mn} \rangle$ 10^{-3} $(a/2)$
100	− 0.057	− 4.49	− 0.056	− 4.44	− 0.051	− 4.06
101	− 0.025	1.77	− 0.026	1.86	− 0.027	1.91
111	0.023	1.81	0.023	1.86	0.024	1.88
200	0.022	− 1.56	0.021	− 1.51	0.022	− 1.54
102	0.011	0.87	0.012	0.94	0.013	1.02
201	− 0.007	− 0.52	− 0.007	− 0.52	− 0.009	− 0.72
112	0.001	− 0.10	− 0.001	0.04	− 0.002	0.15
211	0.007	− 0.51	0.007	− 0.50	0.008	− 0.57
202	0.004	− 0.29	0.004	− 0.27	0.002	− 0.17
122	0.000	0.00	0.002	0.14	0.003	0.24
212	− 0.005	− 0.38	− 0.004	− 0.35	− 0.003	− 0.26
300	− 0.005	− 0.38	− 0.006	− 0.44	− 0.005	− 0.39
103	0.002	− 0.13	0.001	− 0.08	0.002	− 0.10
301	0.008	− 0.54	0.008	− 0.53	0.009	− 0.61
113	− 0.003	− 0.25	− 0.002	− 0.17	− 0.003	− 0.21
311	− 0.007	− 0.57	− 0.007	− 0.52	− 0.007	− 0.54
222	− 0.002	0.15	− 0.002	0.15	− 0.002	0.16
203	0.000	0.00	0.001	0.06	0.001	0.10
302	− 0.001	− 0.10	− 0.002	− 0.12	− 0.002	− 0.17
ℓmn	$\delta_{\ell mn}$	$\langle L^2_{\ell mn} \rangle$ 10^{-4} $(a/2)^2$	$\delta_{\ell mn}$	$\langle L^2_{\ell mn} \rangle$ 10^{-4} $(a/2)^2$	$\delta_{\ell mn}$	$\langle L^2_{\ell mn} \rangle$ 10^{-4} $(a/2)^2$
001	0.001	0.50	0.001	0.45	0.002	0.76
100	0.019	9.32	0.019	9.68	0.024	11.9

The displacement field around a nitrogen vacancy deduced from the $\langle L^{\square\text{-}A}_{\ell mn} \rangle$ in $TiN_{0.82}$ is shown in figure 6 : the nearest titanium atoms ($(a/2, 0, 0)$ position and equivalents) move away from the vacancy, whereas the nearest nitrogen atoms ($(a/2, a/2, 0)$ position and equivalents) move towards the vacancy. The atomic displacement field around a vacancy in $TiN_{0.82}$ is quite similar to that observed in SRO transition metal carbides [26] and to the one calculated by a lattice statics method in the isomorphous compound UC [27].

For this reason, an attempt has been made to calculate static atomic displacements around a nitrogen vacancy in titanium nitride. The formalism previously developed for uranium carbide [27] and based on the Green function method for lattice statics [28] has been used. The elastic constants determined from the phonon spectrum of $TiN_{0.98}$ are given in reference [25]. The experimental and calculated first neighbour atomic displacements are compared in table IV (columms 1 and 2).

The calculated value of the first neighbour titanium displacement is in good agreement with the experimental value. On the other hand the calculated value for the first neighbour

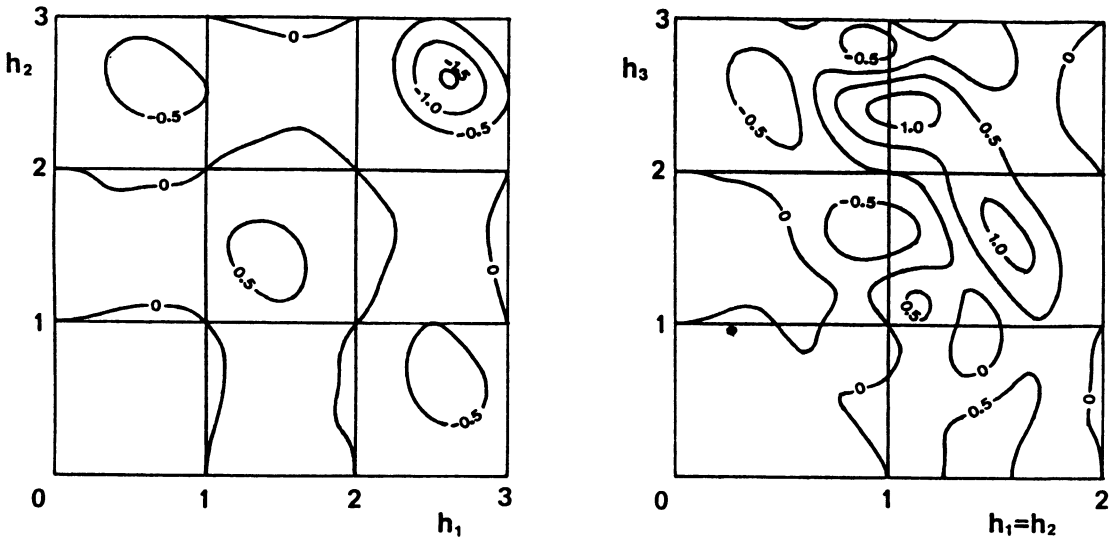

Fig. 5. — First order static displacements contribution to the elastic diffuse intensity ($TiN_{0.82}$, $T = 700$ °C, Laüe units).

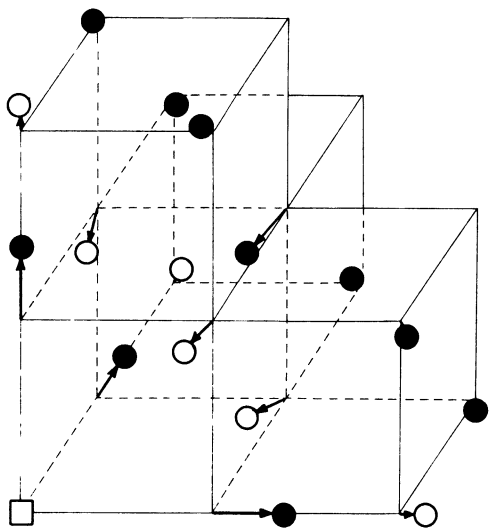

Fig. 6. — Static atomic displacements around a nitrogen vacancy in $TiN_{0.82}$ deduced from the $\gamma_{\ell mn}$ coefficients. (□) : vacancy, (○) : nitrogen, (•) : titanium.

nitrogen displacement differs in sign from the experimental one. This may be due to the fact that only the Ti-Ti and the Ti-N first neighbour elastic constants are known (see [25]).

A more exact evaluation of the atomic displacements around a vacancy requires an estimation of the elastic constants between N-N first neighbours. The latter are connected to the relative variation of lattice parameter $\delta a_{fcc}/a_{fcc}$ induced by metalloid vacancies by a relationship which is given in reference [27] for rocksalt structure carbides and nitrides. For TiN_x, $\delta a_{fcc}/a_{fcc} = 8 \times 10^{-3}\ \delta x$ [29], and this leads to the determination of one of the three N-

N first neighbour elastic constants : $\delta_3' = -0.6$ in $2e^2/a_{fcc}^3$ unit (e : electron charge, for notation see [27]).

The new set of atomic displacements calculated with this value of δ_3' is given in table IV, column 3 : it is in better agreement with experimental data (Tab. IV, column 1).

Table IV. — *Experimental and calculated static atomic displacements around a nitrogen vacancy in* $TiN_{0.82}$ (*in* $a/2$ *units ;* $a/2 = 2.114$ Å).

ℓmn	$\langle L_{\ell mn} \rangle$ experimental ($T = 700$ °C)	$L_{\ell mn}$ calculated with the force constants from [25]	$L_{\ell mn}$ calculated with the force constants from [25] and $\delta_3' = -0.6(2e^2/a_{fcc}^3)$
100 (□-Ti)	+ 0.020	+ 0.016	+ 0.014
101 (□-N)	− 0.008	+ 0.002	− 0.007
200 (□-N)	+ 0.007	+ 0.008	+ 0.007

In fact, the experimental data give the *average* atomic displacements around a vacancy in the largely non-stoichiometric compound TiN_x, whereas in the lattice statics method, one considers the atomic displacements around an *isolated* vacancy in stoichiometric TiN. In the simplest model (additivity of the displacement vectors due to each vacancy), two configurations for the first atomic displacement $L_{100}^{\square\text{-Ti}}$ in TiN_x are obtained :

$$\begin{array}{ccccc} & \text{Ti} & \text{N} & & \\ \square & \times \rightarrow & \bullet & , \quad p_{200}^{\square\text{-N}} = x(1-\alpha_{200}), & L_{100}^{\square\text{-Ti}}(1) = L_{100}^{\square\text{-Ti}} \\ 000 & 100 & 200 & & \end{array} \tag{1}$$

or

$$\begin{array}{ccccc} & \text{Ti} & & & \\ \square & \times & \square & , \quad p_{200}^{\square\text{-}\square} = 1 - x(1-\alpha_{200}), & L_{100}^{\square\text{-Ti}}(2) = 0 \\ 000 & 100 & 200 & & \text{(by symmetry)} . \end{array} \tag{2}$$

The mean atomic displacement $\langle L_{100}^{\square\text{-Ti}} \rangle$ is connected to the displacement $L_{100}^{\square\text{-Ti}}$ induced by an isolated vacancy through the relation :

$$\langle L_{100}^{\square\text{-Ti}} \rangle = p_{200}^{\square\text{-N}} L_{100}^{\square\text{-Ti}}(1) + p_{200}^{\square\text{-}\square} L_{100}^{\square\text{-Ti}}(2) = x(1-\alpha_{200}) L_{100}^{\square\text{-Ti}} .$$

For $x = 0.82$ and $\alpha_{200} = -0.114$, one obtains : $\langle L_{100}^{\square\text{-Ti}} \rangle = 0.91\, L_{100}^{\square\text{-Ti}}$. Therefore the $\langle L_{100}^{\square\text{-Ti}} \rangle$ value calculated by lattice statics for $TiN_{0.82}$ is $0.013\, a_{fcc}/2$ (= 0.028 Å), to be compared to $0.020\, a_{fcc}/2$ (= 0.042 Å) determined experimentally.

5. Short-range-order parameters and effective interatomic ordering energies.

The short-range order contribution $\alpha(\mathbf{Q})$ to the diffuse intensity for $T = 700$ °C (order 0 term) is shown in figure 7a for the two reciprocal planes $\{001\}$ and $\{1\bar{1}0\}$ where the intensity measurements have been carried. In this section, using statistical mechanics, the short-range order parameters are related to the pair interaction energies $V_{\ell mn}$. In a canonical system

(vacancy concentration x fixed), the Hamiltonian which describes the order of vacancies (Ising Hamiltonian) is written as follows :

$$H = V_1 \sum_{i,j^1} C_i C_j + V_2 \sum_{i,j^2} C_i C_j + V_3 \sum_{i,j^3} C_i C_j + V_4 \sum_{i,j^4} C_i C_j \qquad (3)$$

where the sums $\sum_1$, $\sum_2$, $\sum_3$, $\sum_4$ run respectively through the first, second, third and fourth neighbour pairs in the metalloid sublattice. C_i is the occupying factor :

$$C_i = 1 \quad \text{if} \quad i = \text{N}, \quad C_i = 0 \quad \text{if} \quad i = \square ; \qquad V_i = \frac{1}{2} (V_i^{\text{NN}} + V_i^{\square\square} - 2 V_i^{\square\text{N}}) .$$

In this model the pair interactions further than the 4th neighbours are neglected and so are the triplet and other cluster interactions [13].

Three methods are used here to deduce the V_i from the (corrected) measured $\alpha_{\ell mn}$: Clapp and Moss mean field approximation, Monte-Carlo simulations, and inverse Cluster-Variation Method (CVM).

5.1 CLAPP AND MOSS APPROXIMATION. — The Clapp and Moss formula (4) [15, 16] is the simplest mean-field approximation. In this formula, the short-range-order contribution $\alpha(\mathbf{Q})$ to the diffuse intensity is a simple analytic function of the Fourier transform of the interaction potentials $V(\mathbf{Q}) = \sum_{\substack{\ell,m,n \\ \ell+m+n \text{ even}}} V_{\ell mn} \, e^{i\mathbf{Q}\cdot\mathbf{R}_{\ell mn}}$:

$$\alpha(\mathbf{Q}) = \frac{C}{1 + 2x(1-x)\, V(\mathbf{Q})/k_B T} \qquad (4)$$

where

$$C = \left[\frac{1}{v_Q} \int_{v_Q} \frac{d^3\mathbf{Q}}{1 + 2x(1-x)\, V(\mathbf{Q})/k_B T} \right]^{-1}$$

v_Q : first Brillouin zone volume ; k_B is the Boltzmann constant and T the absolute temperature.

From the measured $\alpha(\mathbf{Q})$, a Fletcher and Powell least squares fit method [30] has been used to determine the V_i. The extension of the interaction is assumed to be limited to a few neighbouring shells.

The energies V_i obtained when limiting the interaction to four neighbour shells are given in table V : the first and second neighbour energies V_1 and V_2 are positive and much stronger than the others : $V_1 \simeq 56$ meV, $V_2/V_1 \simeq 0.71$, V_3/V_1 and $V_4/V_1 \lesssim 0.03$. A fit performed with eight energies does not modify V_1 and V_2, but affects somewhat V_3 and V_4 which remain small (see the values given in caption of Tab. V).

The intensity calculated with the Clapp and Moss formula (4) and the V_i of table V is given in figure 7b for $T = 700$ °C. According to the Clapp and Moss maps (Fig. 2), the short-range order for $V_2/V_1 \simeq 0.71$ and $V_3/V_1 \simeq 0.02$ should be of the (1/2 1/2 1/2) type, in agreement with the experimental results (see Fig. 7a).

5.2 MONTE-CARLO SIMULATIONS. — As the measured fluctuations are not very strong in this system, the Monte-Carlo method provides precise values of $\alpha_{\ell mn}$ from known V_i.

The Inverse Linearized Monte-Carlo method described in [31, 32] has been used to determine the V_i.

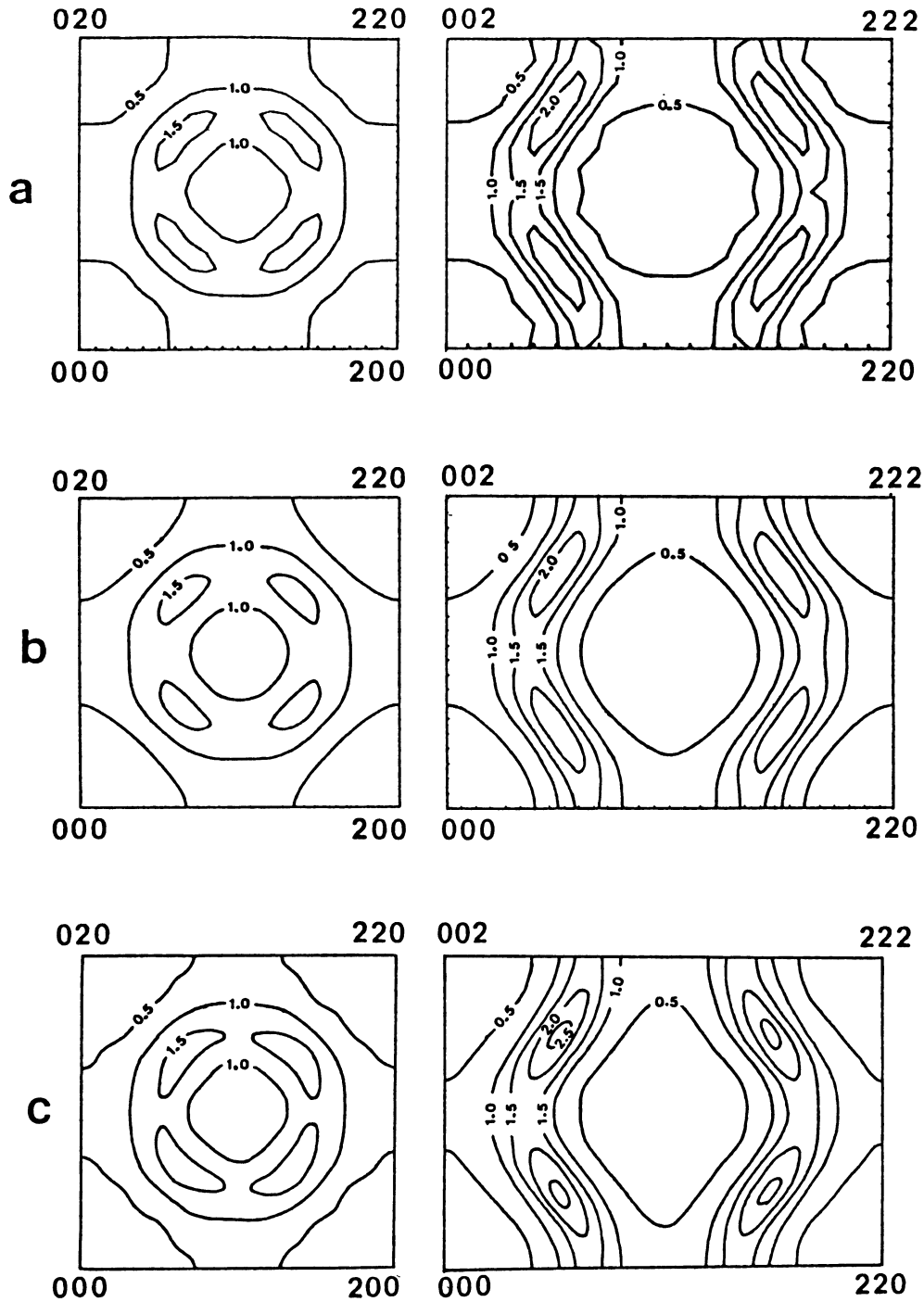

Fig. 7. — Short-range order contribution $d\sigma_{SRO}/d\Omega$ to the elastic diffuse cross-section of $TiN_{0.82}$ at 700 °C in the $\{001\}$ (left) and $\{1\bar{1}0\}$ (right) reciprocal lattice planes (Laüe units). a) Reconstructed from the experimental $\alpha_{\ell mn}$. b) Calculated from Clapp and Moss ordering energies V_i *via* formula (4). c) Calculated from the energies V_i determined by the Monte Carlo method (see Sect. 5.2). d) Calculated from the energies V_i determined by Inverse CVM (see Sect. 5.3).

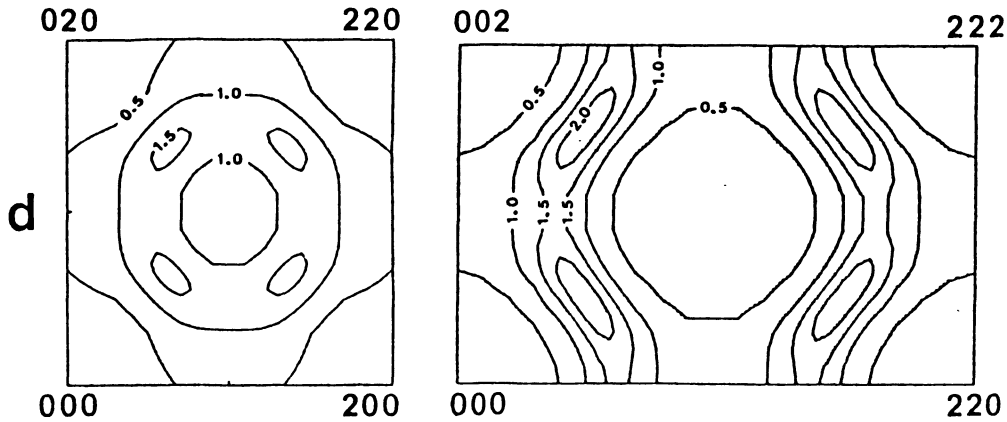

Figure 7 (*continued*).

Table V. — *Mean-field (Clapp-Moss), Inverse Monte Carlo and Inverse* C.V.M. *effective nitrogen-nitrogen ordering energies for the four first neighbour shells in* $TiN_{0.82}$, *calculated from elastic neutron diffuse scattering measurements. The uncertainties deduced from « statistical errors » on* $\alpha_{\ell mn}$ (*Tab.* II) *are given into brackets in the case of* C.V.M. *calculations. The fit by the Clapp and Moss formula* (4) *with* 8 *potentials at* 700 °C *gave :* $V_1 = 57$, $V_2 = 41$, $V_3 = 4$, $V_4 = 5$, $V_5 = 1$, $V_6 = 3$, $V_7 = V_8 = 1$ meV.

	V_i (meV)	T = 700 °C	T = 800 °C	T = 900 °C
Clapp and Moss	V_1	55	56	59
	V_2	39	40	42
	V_3	1	1	2
	V_4	2	2	3
	V_2/V_1	0.71	0.71	0.71
Monte Carlo	V_1	85	82	82
	V_2	64	61	62
	V_3	3	2	4
	V_4	4	4	4
	V_2/V_1	0.75	0.74	0.76
C.V.M.	V_1	90 (6)	87 (6)	87 (6)
	V_2	67 (4)	65 (4)	66 (4)
	V_3	4 (2)	4 (2)	6 (2)
	V_4	5 (1)	5 (1)	6 (1)
	V_2/V_1	0.74	0.75	0.76

•*Calculation from the four first* $\alpha_{\ell mn}$. — Table V shows the results obtained in calculating the four first V_i from the four equations provided by the four first measured $\alpha_{\ell mn}$. The short-range order intensity can be recalculated from these V_i (Fig. 7c) : it appears hardly distinct from the experimental one (Fig. 7a). The set of $\alpha_{\ell mn}$ parameters obtained from these V_i is given in table II column 5. It must be emphasized that although the V_i are obtained from

the four first $\alpha_{\ell mn}$ only, the following $\alpha_{\ell mn}$ parameters are in agreement with the experimental ones (in particular the sign alternance is well reproduced). This result supports the ability of a model hamiltonian with four V_i to describe the measured short-range order.

• *Calculation from the 24 first* $\alpha_{\ell mn}$. — The V_i were also calculated at 700 °C from the 24 $\alpha_{\ell mn}$ given in the first column of table II, by a least-squares fit method (see [31, 32]). The covariance matrix of this least-squares fit leads to an estimate of the range of variation of the V_i which can account for the $\alpha(\mathbf{Q})$. The results are :
$V_1 = 78 \pm 9$ meV, $V_2 = 61 \pm 6$ meV, $V_3 = -2 \pm 3$ meV, $V_4 = 1 \pm 2$ meV, in good agreement with the values from 4 $\alpha_{\ell mn}$ given in table V. A χ^2 test on this fit suggests that the errors on the $\alpha_{\ell mn}$ parameters must be about twice the statistical ones given in table II.

It must be noticed here that if any V_i is changed in the range of error given, the other ones must be also modified. For instance, V_3 and V_4 cannot be let simultaneously to zero.

5.3 CLUSTER VARIATION METHOD RESULTS. — It has long been shown that the CVM [33] is a very precise technique for studying statistical problems in crystalline solids, provided the basic clusters, upon which the algorithm is build, are large enough. Basically, a CVM study consists in minimizing a free energy functional where the exact entropy has been replaced by a linear combination of entropies of finite clusters included in a given basic cluster.

Until recently, most of the CVM studies were done with interactions limited to 1st and 2nd neighbours, and, consequently, with relatively small clusters (up to six points) (for a recent review, see [34]). In the present case, we want to consider pair interactions up to the 4th neighbours. According to an optimized procedure for selecting the basic clusters [35, 36], the smallest clusters that we must use in such a case are the face-centered cube itself, that contains 14 points, and, simultaneously, the 13 point cluster formed by one site surrounded by its twelve first neighbours (see Fig. 8a) ; this approximation is referred to as the 13-14 point

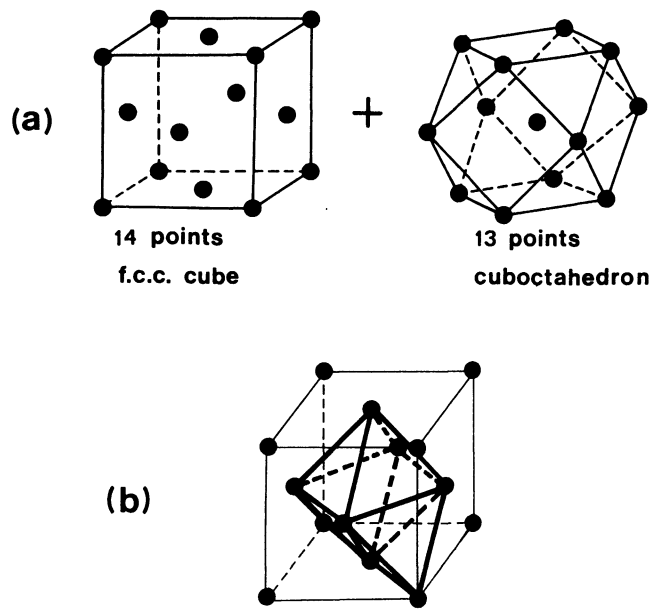

Fig. 8. — Basic clusters for C.V.M. in f.c.c. lattices. a) 13-14 point approximation. b) TO approximation.

approximation. These basic clusters are rather large and lead, in the disordered phase, to a free energy functional which depends on 742 correlation functions.

We have used this 13-14 point approximation in an Inverse CVM algorithm to determine the pair interactions up to V_4. The main steps of that algorithm are as follows [37]. From guessed values $V = (V_1, V_2, V_3, V_4)$ for the pair interactions, a direct minimization of the CVM free energy leads to the correlations included in the 13- and 14-point clusters ; in particular, we calculate the short-range order parameter set $\alpha = (\alpha_1, \alpha_2, \alpha_3, \alpha_4)$. Suppose now that a small variation δV is applied to the set V ; the induced variation $\delta\alpha$ on the set α is given, to first order, by :

$$\delta\alpha = \chi \cdot \delta V$$

where $\chi = \dfrac{\partial\alpha}{\partial V}$ is the generalized susceptibility matrix :

$$\chi_{ij} = \frac{\partial\alpha_i}{\partial V_j}.$$

Hence, if $\Delta\alpha$ is the deviation between the calculated α and the experimental ones,

$$\Delta\alpha = \alpha - \alpha^{\exp}$$

the variation ΔV needed to make up the deviation $\Delta\alpha$ is given, to first order, by the solution of the linear system

$$\chi \cdot \Delta V = \Delta\alpha .$$

The next trial value for the interaction set is then $V + \Delta V$. We stop the process when the deviation $\Delta\alpha$ is smaller than the experimental error. In general, this algorithm converges very rapidly (typically 5 or 6 iterations in V).

We have used this Inverse CVM in the case of $TiN_{0.82}$. The input parameters are the first four measured correlation functions $\alpha_{\ell mn}$. Our results for the three different temperatures are presented in table V where the uncertainties correspond to the statistical errors on $\alpha_{\ell mn}$ given in table II. Note that the calculated interactions do not depend on T, which proves, first, that the short-range order in this system can be precisely described by an Ising model with pair interactions limited to V_4 and, secondly, that the experimental data are very precise. We note also that the CVM results are similar to those obtained by the Inverse Monte-Carlo method.

In order to have a more complete comparison with the experimental data, we have computed, within the CVM framework, the short-range order diffuse intensity, which, in Laue units, is given by $\alpha(\mathbf{Q})$ (the Fourier transform of the coefficients $\alpha(\mathbf{R})$). But, and that point is important, $\alpha(\mathbf{Q})$ has not been computed by a direct Fourier transform of the coefficients $\alpha(\mathbf{R})$ calculated during the CVM minimization, but, instead, by using the fluctuation-dissipation theorem which says that $\alpha(\mathbf{Q})$ is proportional to the staggered susceptibility $\chi(\mathbf{Q})$ (for more details, see [35, 38]). However, due to practical reasons (limitation of computer possibilities, even with a CRAY-XMP), the susceptibility $\chi(\mathbf{Q})$ cannot be computed readily within the 13-14-point approximation. But we remark, at this point, that V_3 and V_4 are much smaller than V_1 and V_2 ($V_3/V_1 \simeq V_4/V_1 \simeq 0.04$) (see Tab. V). Therefore, for the purpose of computing $\chi(\mathbf{Q})$ and as a first approximation, we can use a lower order CVM, namely the tetrahedron-octahedron one (TO) (see Fig. 8b) [39]. More precisely, within the TO approximation, interactions V_1 and V_2 are treated correctly (the associated correlations are inside the basic clusters), whereas V_3 and V_4 are treated in a

mean-field-like way (the corresponding correlations are factorized on the point correlation functions).

We have then computed the short-range order diffuse intensity, *via* $\chi(\mathbf{Q})$ in the TO approximation, with $V_1 = 83$ meV, $V_2 = 62$ meV, $V_3 = 3$ meV, $V_4 = 3$ meV, for the two temperatures $T = 700$ °C and $T = 900$ °C and $x = 0.82$ (Fig. 7d). We can see that these maps are hardly distinct from the experimental ones (Fig. 7a).

5.4 DISCUSSION OF THE APPROXIMATIONS. — The three approximations used here are « self consistent » : in each case, $\alpha(\mathbf{Q})$ can be recalculated with the same approximation and the results are extremely close to the experimental ones.

The uncertainties on the Monte-Carlo V_i were discussed above. We have seen in section 5.2 that the total errors on the $\alpha_{\ell mn}$ are probably about twice the statistical ones given in table II : therefore, the true uncertainties on the V_i calculated by C.V.M. should be twice those given in table V. We also evaluated the effect of normalization errors : at 700 °C, the computed ordering energies varied from $V_1 = 100$ meV, $V_2 = 72$ meV, $V_3 = 7$ meV, $V_4 = 6$ meV from uncorrected $\alpha_{\ell mn}$, to 90, 67, 4 and 5 meV respectively from $\alpha_{\ell mn}$ corrected by formula (2).

In conclusion, the Monte-Carlo and C.V.M. results are in good agreement, V_1 and V_2 being determined with accuracies of approximately ± 10 %.

On the other hand, the Clapp and Moss approximation gives much lower values of V_1 and V_2. This is explained by the strong « frustration » of these interactions in a fcc lattice $A_{1-x}B_x$ (Fig. 9). As the mean-field approximation does not take into account neither the frustration between first neighbour pairs, nor the competition between positive V_1 and V_2, the Clapp and Moss formula tends, for a given set of α parameters, to underestimate the pair interactions. On the other hand, the basic clusters used here in the CVM approximation are large enough to include these frustration effects.

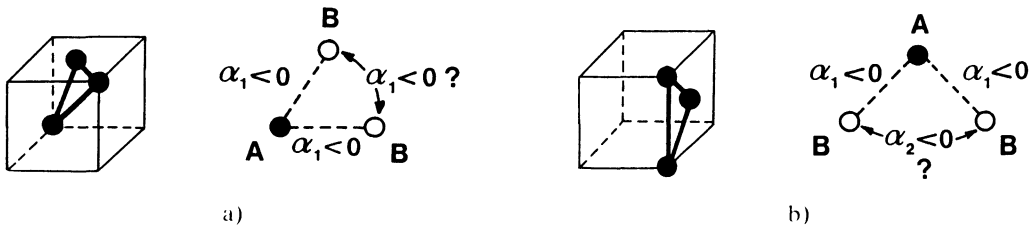

Fig. 9. — Frustration phenomena in a f.c.c. lattice with negative first and second neighbour SRO parameters α_1 and α_2. a) First neighbours. b) Second neighbours.

5.5 DETERMINATION OF THE ORDER TEMPERATURE AND OF THE FUNDAMENTAL STATE. — Finally, we consider now the problem of the critical temperature T_c of the order-disorder transformation.

According to the mean-field approximation (formula (4)), the quantity α^{-1} ($\mathbf{Q} = 1/2\ 1/2\ 1/2$) should be a linear function of $1/T$ and intersect the horizontal axis for the reciprocal spinodal temperature $1/T_s$ (T_s is in fact a lower bound of the order-disorder transition T_c^* that could be determined in the mean-field approximation). Our experimental data give effectively a straight line (see Fig. 10) which, by extrapolation, leads to $T_s = 260$ °C.

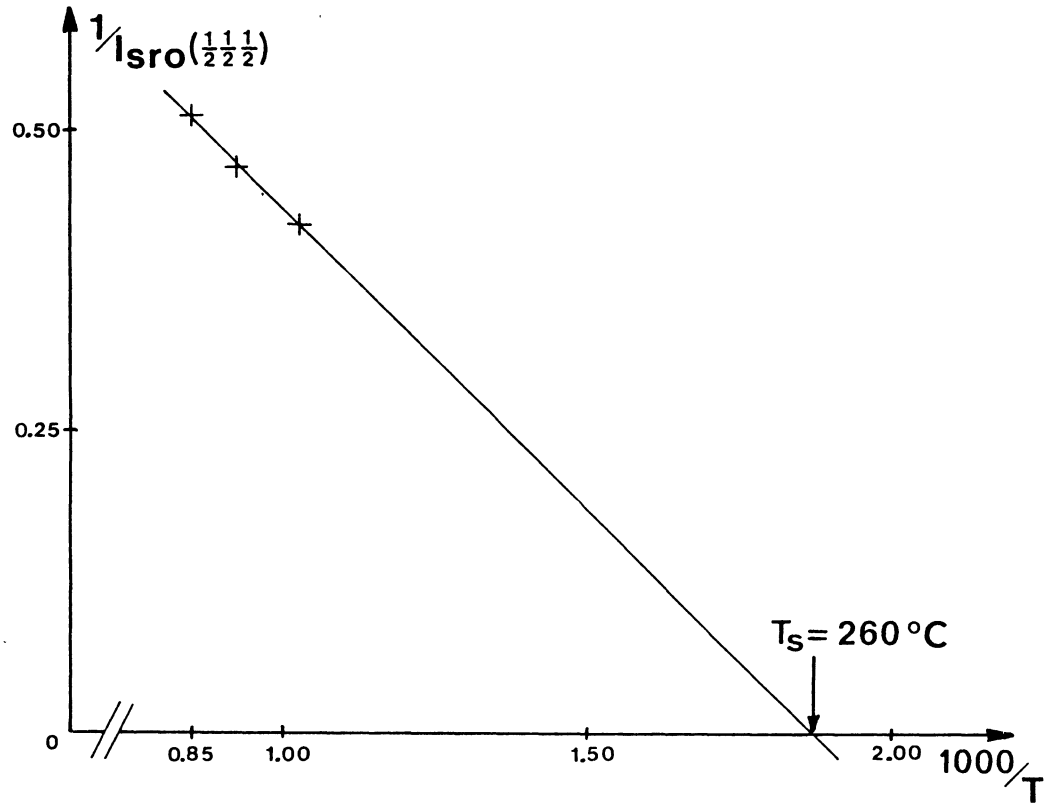

Fig. 10. — Plot of measured $1/I_{SRO}$ (1/2 1/2 1/2) *versus* $1/T$ ($\times 10^3$) in $TiN_{0.82}$.

Using the pair interactions obtained above, it is of course attractive to compute a phase diagram for the Ti-N system around the composition $x = 0.82$. Within the C.V.M. framework, this requires the knowledge of the ground state at $T = 0$. As V_3 and V_4 are very small, this ground state is certainly imposed by interactions V_1 and V_2, whose ratio V_2/V_1 is here equal to 0.73. According to the stability diagram in V_1 and V_2, which is known exactly [40, 41, 42], the ground state for $V_2/V_1 = 0.73$ and around $x = 0.82$ is an A_5B type structure (in the present case, A ≡ nitrogen, B ≡ vacancy). This structure can be described as follows : it consists, along a ⟨110⟩ direction, in a basic sequence of two pure (110) A planes followed by a mixed AB plane and this sequence repeats itself along direction ⟨110⟩ (see Fig. 11). In fact, this A_5B structure is infinitely degenerated, even if V_3 and V_4 are taken into account (for example, three different A_5B LRO structures, degenerated with interactions up to V_4, have been proposed for V_6C_5 and Nb_6C_5 [43, 44]). But at finite temperature, from entropic effects only one A_5B phase should survive (although the free energies of all the A_5B phases are very close together).

Therefore, in order to limit the number of correlation functions, we have chosen to consider, for the C.V.M. phase diagram, the simplest A_5B phase (Fig. 11). In the TO approximation, this phase is defined by 94 correlation functions ([4]) (the use of the TO

([4]) The correlation functions of the A_5B phase have already been listed [45], but, due to an extra approximation these authors found only 76 correlations instead of 94.

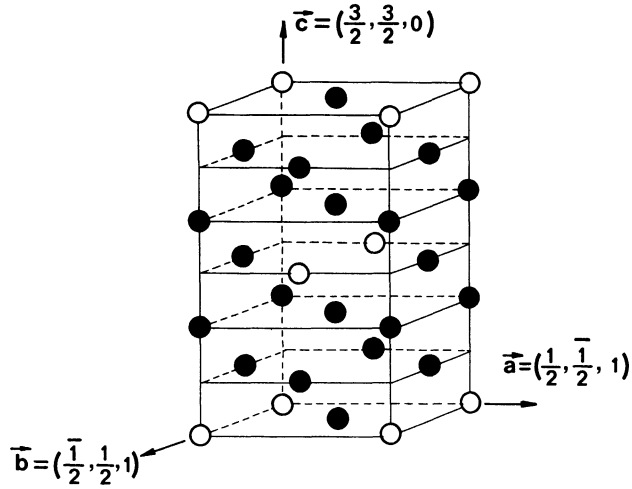

Fig. 11. — A_5B structure (orthorhombic unit cell). (○) : B atoms (vacancy) ; (●) A atoms (nitrogen). **a**// $\langle 1\bar{1}2\rangle_{fcc}$, **b**// $\langle \bar{1}12\rangle_{fcc}$, **c**// $\langle 110\rangle_{fcc}$. For each orthorhombic unit cell vector **a**, **b**, **c**, are indicated its components in the disordered f.c.c. cell.

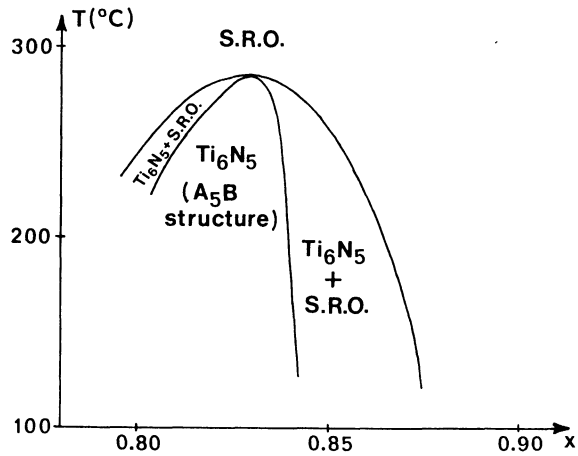

Fig. 12. — TiN_x phase diagram around composition $x \simeq 0.82$, calculated by C.V.M. from $V_1 = 82$ meV and $V_2 = 60$ meV.

approximation has been justified above). The resulting TiN_x phase diagram, around $x = 0.82$, is given in figure 12.

The Monte-Carlo method has been used to simulate the low temperature phase of this system at 460 K with the interaction potentials given in section 5.2 at the A_5B ($\equiv Ti_6N_5\square$) composition. The Monte-Carlo calculated $\alpha_{\ell mn}$ exhibit a long range structure ($\alpha_{\ell mn}$ is not zero at large distance) which is compatible with the A_5B structure until the 28th f.c.c. neighbour shell (see Tab. VI).

Otherwise, the Monte-Carlo critical temperature at heating, $T_C^{0\to D}$, has been found of the order of 600 K ($\simeq 330$ °C) ; the transition is first order and shows a strong hysteresis.

Table VI. — *Values of* $\alpha_{\ell mn}$ *calculated by Monte Carlo simulation for* $TiN_{0.82}$ *in the* LRO *state at* 460 K, *compared to the theoretical values for the perfectly ordered* A_5 B *structure.*

ℓmn	A_5 B structure	M.C. ordered phase
000	1	1
011	− 0.200	− 0.194
002	− 0.200	− 0.194
112	0.200	0.192
022	0.000	0.006
013	0.000	0.000
222	− 0.200	− 0.197
123	− 0.100	− 0.096
004	0.200	0.197
033	0.400	0.382
114	0.000	0.000
024	− 0.200	− 0.197
233	0.000	0.000
224	0.400	0.388
015	0.000	0.000
134	− 0.100	− 0.096
125	0.000	0.000
044	0.000	0.006
035	0.000	0.000
334	0.000	0.000
006	− 0.200	− 0.197
244	− 0.200	− 0.197
116	0.000	0.000
235	− 0.100	− 0.095
026	0.200	0.197
145	0.200	0.191
226	− 0.200	− 0.197
136	0.000	0.000
444	0.400	0.101

In any case, this transition should be very difficult to observe experimentally for kinetic reasons, the nitrogen mean free path for one hour at 285 °C being about 1 Å from atomic diffusion data.

6. Conclusion.

In this work, we have for the first time quantitatively measured short-range order parameters at the equilibrium temperature by neutron diffuse scattering in a refractory non-stoichiometric compound, and determined precise effective ordering interatomic energies.

In $TiN_{0.82}$, vacancies prefer to be on third neighbour positions from a vacancy ($\alpha_{112} > 0$). This property is similar to that found for $VC_{0.75}$ [46] and $NbC_{0.73}$ [26].

Recently, room temperature powder neutron diffraction studies of short-range order were made on $TiN_{0.55}$, $TiN_{0.67}$ and $TiN_{0.75}$ previously annealed at 1 110-1 200 °C [17]. For $TiN_{0.75}$, the SRO parameters found were : $\alpha_{011} = -0.012$, $\alpha_{002} = -0.032$, $\alpha_{112} = -0.006$, $\alpha_{022} = -0.112$, ... These results are inconsistent with ours (especially for α_{112} that we found positive), which may be due to the fact that it is difficult to estimate short-range order parameters from a powder diagram.

We found maxima of diffuse scattering at (1/2 1/2 1/2) and equivalent positions. This is in agreement with the theoretical prediction by Landesman *et al.* [13, 14]. On the other hand, the long-range order observed experimentally in Ti_2N is of the (1 1/2 0) type. The fact that the type of order changes between Ti_2N (long-range order of 1 1/2 0 type) and $TiN_{0.82}$ (short-range order of 1/2 1/2 1/2 type) is probably due to a variation of the pair interactions with composition ; the ratio V_2/V_1 should increase from less than 0.5 for Ti_2N to $\simeq 0.75$ for $TiN_{0.82}$. The generalized perturbation theory predicts the correct trend, but disagrees quantitatively ($V_2/V_1 = 4.2$ for Ti_2N and 6.0 for $TiN_{0.82}$, see [14] and Fig. 1).

The static atomic displacements are similar to those observed in transition metal carbides [26] ; the displacement field calculated by the lattice statics method gives good results if we estimate the missing coefficient δ_3' from the value of $\delta a_{fcc}/a_{fcc}$. These static displacements are not taken into account in the ordering Ising Hamiltonian (3) ; nevertheless, they play probably an important role in the total energy of ordering (in particular they are much larger in Ti_2N than in $TiN_{0.82}$).

We have used three different inverse methods to calculate the pair interactions from the experimental data : the Clapp and Moss formula, the inverse CVM and the Monte-Carlo simulations.

Our first remark is that the results always confirm the calculation of Landesman *et al.* [14] : V_3, V_4 and further potentials are very weak and (although the numerical values disagree with those deduced from Fig. 1) the ordering is dominated by V_1 and V_2 which are positive in the present case. As in transition metal alloys, the effective ordering energies decrease much more rapidly with distance than in normal metal alloys, this damping being due to electron mean free path effects [47].

Secondly, we note that the Clapp and Moss formula leads to interaction ratio V_i/V_1 which are quite good, even if the interactions themselves are not correct. This is due to the fact that the experimental data have been collected at a relatively high temperature ($T \geqslant 700$ °C), in comparison to the order-disorder transition temperature ($T_c = 285$ °C, according to the CVM phase diagram, see Fig. 12). The Clapp and Moss formula has then been used in a regime where it is expected to be relatively precise. This is confirmed by the fact that the plot of α^{-1} ($\mathbf{Q}$ = 1/2 1/2 1/2) *versus* $1/T$, obtained from experimental data, is a straight line, as in the Clapp and Moss formula.

Finally, we note that the calculated interactions do not depend on temperature. This proves, without any ambiguity, that the order-disorder effects in our system are precisely described by an Ising model with pair interactions limited to V_4. Moreover, the good agreement between the CVM and the Monte-Carlo results shows that these two inverse methods are very reliable.

Acknowledgements.

We wish to thank Drs. A.N. Christensen who supplied the $TiN_{0.82}$ single crystal, G. Treglia who calculated the theoretical V_i *versus* N_c curves for M_6N_5 (plotted in Fig. 1), and D. Lesueur for useful discussions. We also acknowledge the staff of Laboratoire Léon Brillouin where the experiments have been performed.

References

[1] TOTH L. E., Transition Metal Carbides and Nitrides (Academic Press, London) 1971.
[2] DE NOVION C. H., LANDESMAN J. P., *Pure Appl. Chem.* **57** (1985) 1391.
[3] BILLINGHAM J., BELL P. S., LEWIS M. H., *Acta Crystallogr.* **A 28** (1972) 602.
[4] NAGAKURA S., KUSUNOKI T., *J. Appl. Cryst.* **10** (1977) 52.
[5] SAUVAGE M., PARTHE E., *Acta Crystallogr.* **A 28** (1972) 607.
[6] OHSHIMA K., HARADA J., MORINAGA M., GEORGOPOULOS P., COHEN J. B., *Acta Crystallogr.* **A 44** (1988) 167.
[7] LOBIER G., MARCON J. P., *C.R. Acad. Sc. Paris Ser. C* **268** (1969) 1132.
[8] CHRISTENSEN A. N., ALAMO A., LANDESMAN J. P., *Acta Crystallogr.* **C 41** (1985) 1009.
[9] ALAMO A., DE NOVION C. H., 7th Int. Conf. on Solid Compounds of Transition Elements, Grenoble (June 1982) paper II-A-1.
[10] HOLMBERG B., *Acta Chem. Scand.* **16** (1962) 1255.
[11] LENGAUER W., ETTMAYER P., *J. Less Common. Met.* **120** (1986) 153.
[12] LENGAUER W., *J. Less Common. Met.* **125** (1986) 127.
[13] LANDESMAN J. P., Report CEA-R-5342 (1986).
[14] LANDESMAN J. P., TREGLIA G., TURCHI P., DUCASTELLE F., *J. Phys. France* **46** (1985) 1001.
[15] CLAPP P. C., MOSS S. C., *Phys. Rev.* **142** (1966) 418.
[16] CLAPP P. C., MOSS S. C., *Phys. Rev.* **171** (1968) 754.
[17] KARIMOV I., PRESMAN V. S., KHVATINSKAYA D. Ya., *Inorg. Mat.* **22** (1986) 199.
[18] PRIEM T., BEUNEU B., DE NOVION C. H., CAUDRON R., SOLAL F., CHRISTENSEN A. N., *Solid State Commun.* **63** (1987) 929.
[19] CHRISTENSEN A. N., *J. Cryst. Growth* **33** (1976) 99.
[20] CAUDRON R., FINEL A., Rapport Technique ONERA n° 11/1221M (1983).
[21] BACON G. E., Neutron Diffraction, 3rd ed. (Oxford University Press, Oxford) 1975.
[22] BLECH J. A., AVERBACH B. L., *Phys. Rev.* **137** (1965) A113.
[23] HOUSKA C. R., *J. Phys. Chem. Solids* **25** (1964) 359.
[24] MOISY-MAURICE V., Report CEA-R-5127 (1981).
[25] KRESS W., ROEDHAMMER P., BILZ M., TEUCHERT W. D., CHRISTENSEN A. N., *Phys. Rev.* **B 17** (1978) 111.
[26] MOISY-MAURICE V., DE NOVION C. H., CHRISTENSEN A. N., JUST W., *Solid State Commun.* **39** (1981) 661.
[27] LESUEUR D., *J. Nucl. Mater.* **102** (1981) 87.
[28] TEWARY V. K., *Adv. Phys.* **22** (1973) 757.
[29] NAGAKURA S., KUSUNOKI T., KARIMOTO F., *J. Appl. Cryst.* **8** (1975) 65.
[30] FLETCHER R., POWELL M. J. D., *Computer J.* **6** (1963) 163.
[31] LIVET F., *Acta Metall.* **35** (1987) 2915.
[32] LIVET F., BESSIERE M., *J. Phys. France* **48** (1987) 1703.
[33] KIKUCHI R., *Phys. Rev.* **81** (1951) 988.
[34] MOHRI T., SANCHEZ J. M., DE FONTAINE D., *Acta Metall.* **33** (1985) 1171.
[35] FINEL A., Thèse de Doctorat d'Etat, Université Pierre et Marie Curie, Paris (1987).
[36] FINEL A., in print in the NATO-ASI Sery on Alloy phase stability, Eds. A. Gonis, G. M. Stocks.
[37] CENEDESE P., FINEL A., GRATIAS D., to be published.
[38] SANCHEZ J. M., *Physica A* **111** (1982) 200.
[39] SANCHEZ J. M., DE FONTAINE D., *Phys. Rev.* **B 21** (1980) 216.
[40] KANAMORI J., *Prog. Th. Phys.* **35** (1966) 16.
[41] SANCHEZ J. M., DE FONTAINE D., Structure and Bonding in Crystals, Vol. II, Eds. M. O'Keefe and A. Navrotsky (Academic Press, New-York) 1981.

[42] KANAMORI J., KAKEHASHI Y., *J. Phys. Colloq. France* **38** (1977) C7-274.
[43] GUSEV A. I., REMPEL A. A., *J. Phys. C.* **20** (1987) 5011.
[44] VENABLES J. D., KAHN D., LYE R. G., *Philos. Mag.* **18** (1968) 177.
[45] SANCHEZ J. M., DE FONTAINE D., *Phys. Rev.* **B 25** (1982) 1759.
[46] SAUVAGE M., PARTHE E., YELON W. B., *Acta Crystallogr.* **A 30** (1974) 597.
[47] DUCASTELLE F., Solid state phase transformations in metals and alloys (Les Editions de Physique, Orsay) 1980, p. 51.